HHS Public Access

Author manuscript

Clin Oncol (R Coll Radiol). Author manuscript; available in PMC 2019 January 12.

Published in final edited form as:

Clin Oncol (R Coll Radiol). 2013 August ; 25(8): 451–460. doi:10.1016/j.clon.2013.05.001.

Functional and Molecular Imaging: Applications for Diagnosis and Staging of Localised Prostate Cancer

B. Turkbey[*], **E. Mena**[*], **O. Aras**[†], **B. Garvey**[*], **K. Grant**[*], and **P.L. Choyke**[*]

[*]Molecular Imaging Program, National Cancer Institute, National Institutes of Health, Bethesda, MD, USA

[†]Department of Radiology, Memorial Sloan-Kettering Cancer Center, New York, NY, USA

Abstract

Prostate cancer is currently the most common solid organ cancer type among men in the Western world. Currently, all decision-making algorithms and nomograms rely on demographics, clinicopathological data and symptoms. Such an approach can easily miss significant cancers while detecting many insignificant cancers. In this review, novel functional and molecular imaging techniques used in the diagnosis and staging of localised prostate cancer and their effect on treatment decisions are discussed.

Keywords

Localization; MRI; PET/CT; prostate cancer; staging

Introduction

Prostate cancer is currently the most common solid organ cancer type among men in the Western world, with a lifetime risk of about one in every six individuals. However, only around one in 36 diagnosed patients will eventually die from prostate cancer [1,2]. Early detection of prostate cancer is important, as treatment of cancer when it is confined to the prostate gland can be curative. However, many prostate cancers are indolent and early diagnosis simply leads to overtreatment. On the other hand, advanced disease can result in increased morbidity, diminished quality of life and death, albeit at a slower rate than most cancers. In the era of prostate-specific antigen (PSA) screening, more patients are being diagnosed with prostate cancer, often of the indolent type. This results from random biopsies of the prostate gland detecting low-grade, microscopic cancer that will take years to grow and may never become symptomatic. One solution to this dilemma is to use imaging to detect only the clinically relevant lesions.

Currently, all decision-making algorithms and nomograms rely on demographics, clinicopathological data and symptoms. However, it is known that such an approach can easily miss significant cancers while detecting many insignificant cancers. Multi-parametric

Author for correspondence: B. Turkbey, Molecular Imaging Program, National Cancer Institute, 10 Center Dr, MSC 1182 Bldg 10, Room B3B69, Bethesda, MD 20892-1088, USA. turkbeyi@mail.nih.gov (B. Turkbey).

magnetic resonance imaging (MP-MRI), which includes both high-resolution anatomic and functional pulse sequences and positron emission tomography–computed tomography (PET/CT) with targeted tracers, has begun to play a major role in the detection and staging of localised prostate cancer [3,4]. In this review, novel functional and molecular imaging techniques used in the diagnosis and staging of localised prostate cancer and their effect on treatment decisions will be discussed.

Multi-parametric Magnetic Resonance Imaging

MP-MRI has greatly improved the identification and staging of localised prostate cancer. With the advent of higher field strength magnets (e.g. 3 Tesla), new coil designs (endorectal and multi-channel phased array surface coils) and imaging sequences, MP-MRI's role has evolved to cancer detection, guided biopsies and therapy. The higher signal derived from modern MRI units enables high-quality scans to be obtained without an endorectal coil, which is considered important for the widespread use of prostate MRI. In this section, four basic parameters comprising a complete MP-MRI will be discussed.

T2-weighted Magnetic Resonance Imaging

T2-weighted MRI is the most commonly used component of MP-MRI of the prostate. It provides superior soft tissue contrast and clear delineation of prostatic zonal anatomy [5–7]. Most prostate cancers are low in T2 signal intensity against a background of high T2 signal intensity of the normal peripheral zone, due to loss of normal glandular morphology with prostate cancer (Figure 1).

However, low T2 signal intensity within the prostate is not always indicative of prostate cancer, as other benign conditions of the prostate, such as prostatitis, benign prostatic hypertrophy (BPH), scars or post-treatment changes (i.e. radiation, hormone ablation), post-biopsy haemorrhage, may have a similar low signal intensity [8,9]. The detection of prostate cancer in the peripheral zone is much easier than in the transitional zone due to coexistence of BPH in the transitional zone. Indicators of tumour in the transitional zone include homogenous low T2 signal intensity without a distinct capsule, ill-defined margins and lenticular shape [6,10].

T2-weighted MRI can also assess whether the tumour is organ confined or extending beyond the prostate capsule. The detection of extracapsular extension (ECE) is quite important for preoperative staging because its presence upstages the patient to T3a stage, and thereby dictates a more aggressive treatment approach. On T2-weighted MRI, ECE usually appears as a direct extension of the tumour into the peri-prostatic fat, but ECE may not be obvious in all conditions; under such circumstances, secondary findings should be sought, including asymmetry of the neurovascular bundle, envelopment of the neurovascular bundle, contour angulation, irregular gland margin, capsular obscuration or retraction and obliteration of the rectoprostatic angle. Seminal vesicle invasion (SVI) can be seen as a low signal defect within the normally high signal seminal vesicles (Figure 2).

T2-weighted MRI alone is reported to have a wide range of sensitivity and specificity for detecting prostate cancer (reported sensitivities: 27–100%; reported specificities 32–99%),

as well as for staging (reported sensitivities 14–100%, reported specificities 67–100%). The wide range of sensitivities and specificities for detection is due to the significant variability of the studied patient populations, as well as differences in the gold standard (biopsy versus surgery) and also depends on the sophistication of the MRI unit and its operator. As a result, the main disadvantage of T2-weighted MRI is that it is highly dependent on the patient and the operator/interpreter [4]. A recent study by Kim *et al.* [11] showed T2-weighted MRI alone at the high field strength (i.e. 3 T) revealing a detection accuracy of 80–90% for tumour foci larger than 1.0 cm in diameter. However, for smaller tumours, T2-weighted MRI was far less accurate [12]. From the standpoint of local staging, particularly with regard to ECE, T2-weighted MRI is considered the most useful technique. In a cohort of 108 patients, Bloch *etal.* [13] evaluated the role of T2-weighted MRI and dynamic contrast-enhanced (DCE) MRI in staging prostate cancer and found an overall sensitivity, specificity, positive predictive value and negative predictive value for ECE of 75, 92, 79 and 91%, respectively. Currently, the presence of overt extension at T2-weighted MRI can be reliably used as an indicator of ECE. However, secondary findings (e.g. bulge, retraction) should be used with caution for making clinical decisions, as they can be falsely positive. T2-weighted MRI is also reported to be a useful technique for the detection of SVI. In a cohort of 573 patients, 28 of whom had SVI, T2-weighted MRI outscored all clinicopathological variables in correctly predicting the SVI with an area under the curve (AUC) of 0.76 (versus 0.62–0.73 for clinicopathological variables) [14]. Calculi or clot within the seminal vesicles as well as unilateral atrophy can mimic SVI. However, combined use of T2-weighted MRI with DCE MRI and diffusion-weighted (DW) MRI is helpful in this setting. In addition to lesion detection and local staging, T2-weighted MRI can also provide information about lesion size, which can be important in choosing the best treatment approach [15]. For example, if the lesion is small (e.g. <5 mm) with no sign of ECE, the patient may be a candidate for active surveillance based on the biopsy results, serum PSA, age and symptomatology. Although MRI is promising, further research is needed to define its role in clinical decision making.

Diffusion-weighted Magnetic Resonance Imaging

DW MRI measures the diffusion (via Brownian motion) of water molecules within the extracellular space [16,17]. Specifically, it measures water proton diffusion with a value called the apparent diffusion coefficient (ADC) [18]. As this property is influenced by cellular density, membrane permeability and extracellular space, DW MRI has the potential to explore some aspects of the microscopic structure of tissue [19,20].

The basis of DW MRI is that stationary water protons (non-diffusing) will not acquire a phase shift when an external magnetic gradient is applied. Moving water protons, on the other hand, will acquire a phase shift proportional to the amount of motion, resulting in loss of signal. If this process is repeated for stronger external magnetic gradients, an estimate of the bulk water diffusion can be made in the form of an ADC map [16]. Due to its higher cellular density, higher nuclear:cytoplasmic ratio and extracellular disorganisation, cancer has significantly restricted water proton diffusion and a hyperintense signal relative to surrounding non-cancerous tissue [21]. Consequently, DW MRI is increasingly used in oncology imaging [22]. Images created by DW MRI at each magnetic gradient strength (or

'b' value) are post-processed to generate ADC values, which are displayed visually as an ADC map. Viable tumours have low ADCs, whereas tumours undergoing therapy are observed to have progressively higher ADCs.

DW MRI can be used to detect prostate cancer due to the lower ADC values of malignant tumours compared with non-cancerous prostate tissue. DW MRI may also yield qualitative and quantitative information for evaluating the therapeutic response in prostate cancer patients throughout and subsequent to radiotherapy, and for predicting locally recurrent prostate cancer post-therapy [23]. Prostate cancers within the peripheral zone are hyperintense relative to a normal peripheral zone on DW MRI and hypointense on ADC maps relative to a normal peripheral zone due to ultrastructural changes mentioned above (Figures 1 and 2). However, DW MRI findings of the transitional zone are more challenging, as the transitional zone is more heterogeneous due to BPH [24,25]. Tumours of both the transitional zone and the peripheral zone have the same appearance on DW MRI and ADC maps. However, detection is confounded by the presence of multiple low signal BPH nodules on ADC maps. Based on diffusion signal alone, such lesions can be confusing, but when placed in the anatomic context of a well-circumscribed BPH nodule as seen on T2-weighted MRI, it becomes easier to differentiate potential malignancy from benign tissue.

The addition of DW MRI to standard imaging protocols dramatically improves the overall diagnostic efficacy of MRI for prostate cancer detection [26]. In a study of 51 patients, Rosenkrantz *et al.* [27] showed that DW MRI and ADC maps had a greater sensitivity than T2-weighted MRI for less experienced readers and improved detection of peripheral zone lesions that were difficult to recognise on T2-weighted MRI.

However, DW MRI has limitations. It has limited spatial resolution, which is critical for local staging. It is also prone to susceptibility artefacts, especially those caused by rectal gas lying against the prostate.

Recently, ADC values of prostate cancer foci were correlated with Gleason scores [28,29]. Turkbey *et al.* [29] reported a negative correlation between tumour ADC values and Gleason scores in 48 patients scanned at 3 T. Moreover, they reported utility of ADC values in predicting D'Amico clinical risk scores. The ability to predict tumour aggressiveness is useful in selecting appropriate therapies and DW MRI is thus far the most promising quantitative MRI technique for accomplishing this non-invasively. However, there remains overlap between Gleason scores and ADC values, thus limiting DW MRI's predictive value in individual patients. Moreover, not all lesions found to have low ADC values are actually tumours. This underscores the need to obtain biopsies in patients with suspected lesions on MRI regardless of their ADC value.

Magnetic Resonance Spectroscopic Imaging

Proton magnetic resonance spectroscopic imaging (MRSI) is a functional method used to assess prostate tissue metabolism. Each volume of interest (voxel) acquired in a three-dimensional MRSI contains a metabolite spectra demonstrating the relative concentrations of metabolites such as citrate, creatine and choline. Prostate tumours are characterised by increased levels of choline and decreased levels of citrate, whereas normal prostate tissues

contain high levels of citrate and relatively low levels of choline and creatine. Thus, increases in the ratios (choline + creatine)/citrate and choline/citrate are a marker for prostate cancer [30] (Figure 1).

MRSI has been studied for several decades, and its joint use with T2-weighted MRI has been shown to aid in tumour volume estimation [31] and tumour localisation [32–34]. However, a recent prospective multicentre study carried out by the American College of Radiology Imaging Network (ACRIN) to determine the benefit of combined endorectal MRI and MRSI concluded that T2-weighted MRI alone and combined T2-weighted MRI–MRSI had similar accuracy in peripheral zone cancer localisation (AUC, 0.60 versus 0.58, respectively; $P > 0.05$). AUCs for individual readers were 0.57–0.63 for T2-weighted MRI alone and 0.54–0.61 for combined T2-weighted MRI–MRSI, without significant difference [35]. On the other hand, in a recent study by Selnaes *et al.* [36], the authors used a stringent segmental matching of histopathology and MRI. They found that combined T2-weighted MRI–MRSI performed better than T2-weighted imaging alone, with AUCs of 0.90 versus 0.85. A principal advantage of the addition of MRSI to MP-MRI is its specificity [37]. There is growing recognition of the importance of identifying clinically significant tumours and differentiating them from lower grade tumours that may have no impact on the patient's longevity [38]. Multiple authors have incorporated MRSI into nomograms to help predict the aggressiveness of tumours [39,40].

Several investigators have noted a correlation between metabolic ratios (e.g. choline/citrate) and prostate cancer aggressiveness [41–43]. Recently, Kobus *et al.* [44] studied the performance of MRSI alone and in combination with ADCs of DW imaging at 3 T. In this study, 54 patients with biopsy-proven cancer underwent MRSI before prostatectomy. They found a significant correlation between aggressiveness classes and (choline + creatine)/citrate ratio, choline/citrate ratio, and ADC values in peripheral zone tumours with AUCs of 71, 67 and 81%, respectively. Furthermore, they found a significant correlation between aggressiveness classes and (choline + creatine)/citrate ratio and choline/citrate ratio in the transitional (rho = 0.58 and 0.60, respectively). Thus, the authors confirmed the potential of MRSI in the assessment of prostate cancer aggressiveness. However, further validation is needed [44].

Because of its reduced spatial resolution compared with other modalities, MRSI would not be expected to be helpful in detecting ECE. Nevertheless, Yu *et al.* [45] reported that the addition of MRSI to MRI improved the diagnostic accuracy for ECE among less experienced readers. They used the location and number of abnormal MRSI voxels for the evaluation of ECE. In this study, patients with the least extensive tumours on MRSI (<1 cancer voxel per section) were found to have a 6% risk for ECE, whereas patients with the most extensive tumours (>4 cancer voxels per section) had an 80% risk of ECE. However, despite these favourable results, MRSI is not used for local staging and mainly serves to confirm aggressiveness of lesions detected in other MP-MRI sequences.

MRSI is both technically challenging and time consuming, adding to the expense of MRI studies. Most vendors now supply a workable MRSI package for prostate imaging. However, proper performance of the scan is still needed, such as proper magnetic resonance shimming.

Partial volume effects, owing to the large size of the MRSI voxel, may be misinterpreted by less experienced readers. MRSI requires additional time for post-processing, decreasing clinical throughput and requiring skilled labour. For these reasons, proton MRSI has not gained the widespread clinical use that other MP-MRI sequences have achieved.

Dynamic Contrast-enhanced Magnetic Resonance Imaging

DCE MRI is an important functional sequence in prostate cancer imaging. DCE MRI involves the acquisition of sequential images using fast T1-weighted sequences before, during and after the injection of an MRI contrast agent (such as low molecular weight gadolinium chelates) within the prostatic tissue. DCE MRI has high sensitivity, which can be useful for the initial evaluation of potential tumour foci, and has been routinely used to detect lesions and cancer aggressiveness, and to monitor therapeutic responses in clinic trial settings. It uses rapid T1-weighted sequences to detect the arrival and uptake of the contrast agent before it washes out. DCE MRI provides a rough delineation of perfusion and permeability in different regions of the prostate [46,47]. Tumour enhancement is often earlier, more rapid and with a more rapid washout, than normal tissue because the highly permeable vessels found in tumours, termed neoangiogenesis, are thought to be related to tumour aggressiveness [48] (Figures 1 and 2). However, abnormal enhancement patterns can be seen in BPH nodules and inflammation, making assessment of the central gland difficult [49]. Furthermore, smaller and low-grade tumour foci frequently do not show abnormal enhancement on DCE MRI [50].

The most common evaluation method for DCE MRI is the qualitative approach, which is the visual detection of focal early and intense enhancement with early washout compared with normal prostatic tissue. Additionally, pharmacokinetic parameters (K^{trans} [transfer of gadolinium contrast from the vascular compartment to the tumour compartment, representing forward vascular permeability and flow], k_{ep} [reverse transfer of contrast from the extracellular space back to the plasma space, representing backward leakage]) can be determined semi-quantitatively, using different kinetic models that provide indices of vascular permeability [51]. Newer software is able to generate these curves along with colour maps for easier interpretation. Semi-quantitative analysis is based on fitting the time–gadolinium concentration curve to the two compartment model. In addition to these calculated permeability parameters, the time–gadolinium concentration curve can be used to measure the AUC, the time to peak enhancement and the initial slope. Enhancement curves can be classified into one of three types: type 1, persistent increase; type 2, plateau curve; and type 3, decline after initial upslope. Of these curves, type 3 is most commonly associated with prostate cancer, although mixtures of different curves are often found within lesions [52].

For the detection of tumours, DCE MRI alone has a sensitivity and specificity range of 46–96% and 74–96%, respectively. However, these ranges are highly dependent on patient selection, image acquisition and analysis technique, lesion size and diagnostic criteria [4]. A recent work by Puech *et al.* [53] analysed the performance of DCE MRI (at 1.5 T) in identifying and localising intraprostatic cancer foci in relation to cancer volume at histology. The sensitivity and specificity of DCE MRI for the identification of tumour foci of any

volume were 32 and 95%, respectively. For the identification of tumour foci >0.5 ml, the sensitivity and specificity were 86 and 94%, respectively, and the AUC was 0.874 [53].

The transitional zone is a challenging area for tumour detection, as BPH nodules often show early and intense enhancement, much like tumours. However, similar to tumours in the peripheral zone, transitional zone tumours also show early washout, which is unusual in BPH nodules. Nonetheless, it is important to interpret DCE MRI of the transitional zone in the context of the T2-weighted results. BPH nodules can often be distinguished by a clear capsular demarcation and a rounded appearance. It is uncommon for a BPH nodule to contain cancer. Thus, lesions that seem to be BPH nodules on T2-weighted MRI can be disregarded, irrespective of their appearance on DCE MRI [54,55].

DCE MRI suffers from a relatively lower spatial resolution, so it must be combined with T2-weighted MRI to improve prostate cancer detection and local staging (AUC 95% overall staging accuracy), compared with each technique alone [56,57]. DCE MRI plays a key role in confirming a suspicion of SVI detected via T2-weighted MRI and/or DW MRI. The presence of early enhancement within a suspected seminal vesicle lesion strongly suggests invasion. Ogura *et al.* [58] reported that early, intense enhancement of the seminal vesicles has an accuracy rate of 97% for SVI.

DCE MRI is the most important magnetic resonance sequence in the detection of cancer recurrence after previous treatment of prostate cancer, especially after prostatectomy, focal ablation and radiotherapy, as other magnetic resonance methods are affected by treatment-related anatomical and functional changes, such as surgical clips, fiducial markers and fibrosis.

Positron Emission Tomography/Computed Tomography

The strengths of MRI lie in its highly detailed anatomy, multi-parametric acquisition, lack of ionising radiation and widespread availability. However, PET is significantly more sensitive than MRI. PET achieves this sensitivity at the expense of resolution; although, to some extent this can be compensated for by fusing the PET and CT data (PET/CT). PET has the ability to image tumour-specific biochemical and metabolic alterations, such as increased glucose metabolism, increased protein and DNA synthesis, increased lipid metabolism and altered receptor phenotypes, by using the proper PET radioactive drug. Numerous novel PET radiotracers are currently under investigation for prostate cancer imaging (discussed below).

The most common PET radiotracer used in clinical studies is a fluorine-18 labelled glucose analogue, ^{18}F-fluorodeoxyglucose (FDG), which is an indicator of glycolysis in cancer cells. Experience has shown that ^{18}F-FDG is not useful in the initial diagnosis and staging of prostate cancer because lower grade prostate cancers do not depend principally on glycolysis for growth. This results in a low expression of GLUT1 transporters in these slow-growing tumours [59,60]. Meanwhile, FDG is avidly taken up by prostatic tissue in non-malignant conditions such as BPH and prostatitis [61–64]. In addition, the physiological excretion of FDG into the urinary system can limit the evaluation of the prostate due to intense activity in

the bladder, which may mask the primary prostate tumour site or locoregional lymph node metastases. Mixed results have been reported for FDG in organ-confined prostate cancer. In the earliest literature, Effert *et al.* [60] reported a low uptake of ^{18}F-FDG in 81% of untreated, primary prostate tumours without any correlation between uptake and tumour grade or stage. By contrast, recent publications, using newer PET cameras and PET/CT combination, have suggested that ^{18}F-FDG may reflect the prostate tumour biology by showing accumulation in more aggressive lesions compared with indolent lesions, with sensitivity up to 80% in tumour detection when grouping higher Gleason score lesions [65,66]. However, the overlap of tracer FDG accumulation in prostate tumours and BPH remains a limitation for tumour characterisation. Because ^{18}F-FDG PET does not meet all the clinical needs for prostate cancer imaging, a wide variety of alternative PET tracers have been developed for prostate cancer over the last decade.

^{11}C-acetate is a PET radiotracer believed to become incorporated into the cell membrane lipids of prostate tumour cells due to the dominance of fatty acid metabolism[67]. Because ^{11}C-acetate is excreted mostly via the pancreas, imaging of the pelvis is potentially suitable with this tracer. A major limitation is the short half-life of ^{11}C ($T_{1/2}$ ~ 20 min), which requires an on-site cyclotron. When ^{11}C-acetate was compared with ^{18}F-FDG by Oyama *et al*[68]., they concluded that ^{11}C-acetate was more sensitive than ^{18}F-FDG for the detection of primary prostate tumours. However, other studies have reported an overlap of ^{11}C-acetate uptake between malignant and non-malignant prostatic tissue [69]. In a recent study, Mena *et al.* [70] compared MP-MRI and ^{11}C-acetate PET/CT in localised prostate carcinoma, with whole mount section histopa-thology. They reported a sensitivity and specificity of 61.6 and 80.0% for ^{11}C-acetate and 82.3 and 95.1%, for MP-MRI; ^{11}C-acetate uptake correlated with neither Gleason score nor PSA values [70]. Similarly, Jambor *et al.* [71] found that ^{11}C-acetate PET was unable to provide information on cancer aggressiveness. Despite the uptake overlap between prostate cancer and BPH nodules, ^{11}C-acetate can be potentially used to monitor disease status after focal therapy, surgery or radiation, and this needs further research (Figure 3).

Choline PET radiotracers have also been investigated for prostate cancer imaging. These are based on the presence of choline kinase in malignant tissue, which is involved in lipid and cholesterol metabolism and transport [72]. Choline can be radiolabelled with either ^{11}C (^{11}C-choline) or ^{18}F (^{18}F-fluoromethylcholine, FCH). These radiotracers have shown conflicting results for the detection of primary prostate cancer; some investigators have reported high sensitivity of 87% for ^{11}C-choline [73], even higher than MRI and MRSI (100% versus 60% versus 65%) [74], whereas other studies have reported lower sensitivity of 66% [75] and even lower sensitivity relative to MRSI (55% versus 81%) [76]. Sensitivity may depend on several factors, such as tumour grade, size or location [77,78]. On the other hand, similar to ^{11}C-acetate, ^{11}C-choline and ^{18}F-fluorocholine uptake overlaps among cancer and normal prostatic tissue or BPH [79,80] and uptake does not correlate with tumour grade, PSA, Gleason score, tumour volume [81] or with cellular proliferation [82]. However, ^{11}C-choline PET has the potential for the detection of cancer after biochemical recurrence after therapy. ^{11}C-choline performed better than clinical nomograms in predicting nodal metastases and showed a sensitivity of 93% for detecting local recurrence or distant metastasis [83]. The sensitivity seemed to correlate positively with serum PSA level [84,85].

Looking to the future, however, the limited availability of ^{11}C production means that for choline agents to be successful, they must migrate to labelling with ^{18}F, which has a longer half-life. Unfortunately, this chemical alteration results in more renal excretion, leading to bladder activity artefacts.

The amino acid transport metabolism is an important method for prostate cancers to generate energy and find substrates for protein synthesis. One of the earliest investigated amino acid-based PET tracers was ^{11}C-methionine. ^{11}C-methionine PET seemed to be useful in detecting primary prostate tumours of both low and high Gleason scores [86] and it has been shown to be superior to FDG in identifying metastatic disease [87]. Another amino acid PET tracer is ^{18}F-fluorocyclobutane-1-carboxylic acid (FACBC), a synthetic L-leucine amino acid analogue whose uptake by prostate carcinoma cells is probably mediated by sodium-independent L-type large-neutral amino acid transport system. Initial experience with anti-^{18}F-FACBC was reported in primary (n = 9) and suspected recurrence (n = 6) prostate cancer by Schuster *et al.* [88]. More recently, the same group [89] reported a sensitivity, specificity and accuracy of 81.3, 50.0 and 70.8%, respectively, to localise prostate tumour in a cohort of 10 patients; no significant correlation was seen between anti-^{18}F-FACBC uptake and Ki-67, a proliferation marker. Furthermore, there was no distinct separation between malignant and non-malignant sextants or between Gleason score level and uptake of anti-^{18}F-FACBC. Turkbey *etal.* [90] also reported an overlap of anti-^{18}F-FACBC uptake with non-malignant histology in organ-confined prostate cancer. Despite its limited value in localised prostate cancer, ^{18}F-FACBC is a useful probe for treatment follow-up and more locoregionally advanced disease. In the setting of biochemical recurrence, Schuster *et al.* [91] reported suboptimal specificity of anti-^{18}F-FACBC in the prostate bed, but very promising results in the detection of occult extraprostatic sites of disease.

Prostate-specific membrane antigen (PSMA) has also emerged as a candidate imaging biomarker for prostate cancer. The current commercially available anti-PSMA antibody tracer, ^{111}In-labelled capromab pendetide (ProstaScint®), targets the internal domain of the PSMA receptor and, thus, only apoptotic or necrotic tissue is accessible to the agent. ProstaScint has shown suboptimal sensitivity and specificity in imaging the prostate fossa and detecting osseous metastases [92]. Although this agent is not used for detecting localised prostate cancer, other radiolabelled molecules that bind to the extracellular domain of PSMA have recently emerged for single-photon emission computed tomography (SPECT) imaging use; ^{123}I-MIP-1072 is one such agent that is currently under development. Similarly, a ^{99m}Tc-labelled version of this agent is undergoing testing [93]. A PET agent similar to these small molecule SPECT agents is ^{18}F-DCFBC, which has shown promising results for the detection of metastatic prostate cancer [94], but has not been used extensively in localised disease.

A major limitation of the aforementioned agents is that they have not been tested in large multicentre studies. PET imaging is expensive, and only a few institutions are capable of synthesising agents. Moreover, incentives in academics favour the development of novel PET agents rather than the multicentre testing of existing agents. The assessment of prostate cancer imaging remains a challenge in many clinical situations for PET imaging and the ‘dream’ PET tracer has yet to be discovered. It is hoped that these advances in molecular

imaging may provide new insights into prostate cancer biology that will translate into better treatment planning and thereby contribute to long-term reductions in the morbidity and mortality of prostate cancer.

Conclusion

Accurate detection and local staging of prostate cancer is important for delivering optimal treatment to the patient. Novel imaging techniques, such as MP-MRI and PET/CT with targeted radiotracers, are promising methods. MP-MRI is much further ahead. It has the ability to detect clinically significant intraprostatic tumours and can provide valuable information about local staging and tumour aggressiveness. PET/CT has not yet made a clinical impact in localised prostate cancer, but the growing number of novel tracers augers well for the future of prostate cancer detection. So far, a common limitation of the current PET agents is overlap of uptake between tumour and non-tumoral pathologies, and some agents excreted by the kidney obscure the prostate. PET/CT promises to be useful in the setting of local tumour recurrence. Continued research is required to optimise these novel imaging techniques and implement them into routine clinical practice.

Acknowledgements

This publication was made possible in part by a Pelican Fellowship grant to Dr Omer Aras, supported by The Peter Michael Foundation.

References

[1]. Jemal A, Bray F, Center MM, Ferlay J, Ward E, Forman D. Global cancer statistics. CA Cancer J Clin 2011;61:69–90. [PubMed: 21296855]

[2]. Siegel R, Naishadham D, Jemal A. Cancer statistics. CA Cancer J Clin 2012;2012(62):10–29.

[3]. Turkbey B, Bernardo M, Merino MJ, Wood BJ, Pinto PA, Choyke PL. MRI of localized prostate cancer: coming of age in the PSA era. Diagn Interv Radiol 2012;18:34–45. [PubMed: 21922459]

[4]. Bouchelouche K, Turkbey B, Choyke P, Capala J. Imaging prostate cancer: an update on positron emission tomography and magnetic resonance imaging. Curr Urol Rep 2010;11: 180–190. [PubMed: 20425625]

[5]. Turkbey B, Pinto PA, Mani H, et al. Prostate cancer: value of multiparametric MR imaging at 3 T for detection — histopathologic correlation. Radiology 2010;255:89–99. [PubMed: 20308447]

[6]. Akin O, Sala E, Moskowitz CS, et al. Transition zone prostate cancers: features, detection, localization, and staging at endorectal MR imaging. Radiology 2006;239:784–792. [PubMed: 16569788]

[7]. Ravizzini G, Turkbey B, Kurdziel K, Choyke PL. New horizons in prostate cancer imaging. Eur J Radiol 2009;70:212–226. [PubMed: 18993004]

[8]. Sala E, Eberhardt SC, Akin O, et al. Endorectal MR imaging before salvage prostatectomy: tumor localization and staging. Radiology 2006;238:176–183. [PubMed: 16373766]

[9]. Hom JJ, Coakley FV, Simko JP, et al. Endorectal MR and MR spectroscopic imaging of prostate cancer: histopathological determinants of tumor visibility. AJR Am J Roentgenol 2005;184(Suppl. 4):S62. [PubMed: 15728024]

[10]. Vargas HA, Akin O, Franiel T, et al. Normal central zone of the prostate and central zone involvement by prostate cancer: clinical and MR imaging implications. Radiology 2012;262: 894–902. [PubMed: 22357889]

[11]. Kim CK, Park BK, Kim B. Localization of prostate cancer using 3T MRI: comparison of T2-weighted and dynamic contrast-enhanced imaging. J Comput Assist Tomogr 2006;30:7–11. [PubMed: 16365565]

[12]. Nakashima J, Tanimoto A, Imai Y, et al. Endorectal MRI for prediction of tumor site, tumor size, and local extension of prostate cancer. Urology 2004;64:101–105. [PubMed: 15245944]

[13]. Bloch BN, Genega EM, Costa DN, et al. Prediction of prostate cancer extracapsular extension with high spatial resolution dynamic contrast-enhanced 3-T MRI. Eur Radiol 2012;22: 2201–2210. [PubMed: 22661019]

[14]. Wang L, Hricak H, Kattan MW, et al. Prediction of seminal vesicle invasion in prostate cancer: incremental value of adding endorectal MR imaging to the Kattan nomogram. Radiology 2007;242:182–188. [PubMed: 17090712]

[15]. Turkbey B, Mani H, Aras O, et al. Correlation of magnetic resonance imaging tumor volume with histopathology. J Urol 2012;188:1157–1163. [PubMed: 22901591]

[16]. Lawrence EM, Gnanapragasam VJ, Priest AN, et al. The emerging role of diffusion-weighted MRI in prostate cancer management. Nat Rev Urol 2012;9:94–101. [PubMed: 22249194]

[17]. Morgan VA, Riches SF, Giles S, et al. Diffusion-weighted MRI for locally recurrent prostate cancer after external beam radiotherapy. AJRAm J Roentgenol 2012;198:596–602.

[18]. Panebianco V, Sciarra A, Marcantonio A, et al. Conventional imaging and multiparametric magnetic resonance (MRI, MRS, DWI, MRP) in the diagnosis of prostate cancer. QJ Nucl Med Mol Imaging 2012;56:331–342.

[19]. Tan CH, Wei W, Johnson V, et al. Diffusion-weighted MRI in the detection of prostate cancer: meta-analysis. AJR Am J Roentgenol 2012;199:822–829. [PubMed: 22997374]

[20]. Wu LM, Xu JR, Gu HY, et al. Usefulness of diffusion-weighted magnetic resonance imaging in the diagnosis of prostate cancer. Acad Radiol 2012;19:1215–1224. [PubMed: 22958718]

[21]. Lim KS, Tan CH. Diffusion-weighted MRI of adult male pelvic cancers. Clin Radiol 2012;67:899–908. [PubMed: 22498730]

[22]. Turkbey B, Choyke PL. Multiparametric MRI and prostate cancer diagnosis and risk stratification. Curr Opin Urol 2012;22:310–315. [PubMed: 22617060]

[23]. Iraha Y, Murayama S, Kamiya A, et al. Diffusion-weighted MRI and PSA correlations in patients with prostate cancer treated with radiation and hormonal therapy. Anticancer Res 2012;32:4467–4472. [PubMed: 23060574]

[24]. Oto A, Kayhan A, Jiang Y, et al. Prostate cancer: differentiation of central gland cancer from benign prostatic hyperplasia by using diffusion-weighted and dynamic contrast-enhanced MR imaging. Radiology 2010;257:715–723. [PubMed: 20843992]

[25]. Tamada T, Sone T, Toshimitsu S, et al. Age-related and zonal anatomical changes of apparent diffusion coefficient values in normal human prostatic tissues. J Magn Reson Imaging 2008;27:552–556. [PubMed: 18219616]

[26]. Rinaldi D, Fiocchi F, Ligabue G, et al. Role of diffusion-weighted magnetic resonance imaging in prostate cancer evaluation. Radiol Med 2012;117:1429–1440. [PubMed: 22580813]

[27]. Rosenkrantz AB, Chandarana H, Gilet A, et al. Prostate cancer: utility of diffusion-weighted imaging as a marker of side-specific risk of extracapsular extension. J Magn Reson Imaging 2012 (online first).

[28]. Hambrock T, Somford DM, Huisman HJ, et al. Relationship between apparent diffusion coefficients at 3.0-T MR imaging and Gleason grade in peripheral zone prostate cancer. Radiology 2011;259:453–461. [PubMed: 21502392]

[29]. Turkbey B, Shah VP, Pang Y, et al. Is apparent diffusion coefficient associated with clinical risk scores for prostate cancers that are visible on 3-T MR images? Radiology 2011;258: 488–495. [PubMed: 21177390]

[30]. Jung JA, Coakley FV, Vigneron DB, et al. Prostate depiction at endorectal MR spectroscopic imaging: investigation of a standardized evaluation system. Radiology 2004;233: 701–708. [PubMed: 15564406]

[31]. Coakley FV, Kurhanewicz J, Lu Y, et al. Prostate cancer tumor volume: measurement with endorectal MR and MR spectroscopic imaging. Radiology 2002;223:91–97. [PubMed: 11930052]

[32]. Shukla-Dave A, Hricak H, Moskowitz C, et al. Detection of prostate cancer with MR spectroscopic imaging: an expanded paradigm incorporating polyamines. Radiology 2007;245:499–506. [PubMed: 17890357]

[33]. Scheidler J, Hricak H, Vigneron DB, et al. Prostate cancer: localization with three-dimensional proton MR spectroscopic imaging-clinicopathologic study. Radiology 1999;213:473–480. [PubMed: 10551229]

[34]. Futterer JJ, Heijmink SW, Scheenen TW, et al. Prostate cancer localization with dynamic contrast-enhanced MR imaging and proton MR spectroscopic imaging. Radiology 2006;241: 449–458. [PubMed: 16966484]

[35]. Weinreb JC, Blume JD, Coakley FV, et al. Prostate cancer: sextant localization at MR imaging and MR spectroscopic imaging before prostatectomy-results of ACRIN prospective multi-institutional clinicopathologic study. Radiology 2009;251:122–133. [PubMed: 19332850]

[36]. Selnaes KM, Heerschap A, Jensen LR, et al. Peripheral zone prostate cancer localization by multiparametric magnetic resonance at 3 T: unbiased cancer identification by matching to histopathology. Invest Radiol 2012;47:624–633. [PubMed: 23011187]

[37]. Turkbey B, Mani H, Shah V, et al. Multiparametric 3T prostate magnetic resonance imaging to detect cancer: histopatho-logical correlation using prostatectomy specimens processed in customized magnetic resonance imaging based molds. J Urol 2011;186:1818–1824. [PubMed: 21944089]

[38]. Ploussard G, Epstein JI, Montironi R, et al. The contemporary concept of significant versus insignificant prostate cancer. Eur Urol 2011;60:291–303. [PubMed: 21601982]

[39]. Shukla-Dave A, Hricak H, Akin O, et al. Preoperative nomograms incorporating magnetic resonance imaging and spectroscopy for prediction of insignificant prostate cancer. BJU Int 2012;109:1315–1322. [PubMed: 21933336]

[40]. Westphalen AC, Koff WJ, Coakley FV, et al. Prostate cancer: prediction of biochemical failure after external-beam radiation therapy-Kattan nomogram and endorectal MR imaging estimation of tumor volume. Radiology 2011;261:477–486. [PubMed: 21873255]

[41]. Kobus T, Hambrock T, Hulsbergen-van de Kaa CA, et al. In vivo assessment of prostate cancer aggressiveness using magnetic resonance spectroscopic imaging at 3 T with an endorectal coil. Eur Urol 2011;60:1074–1080. [PubMed: 21419565]

[42]. Scheenen TW, Heijmink SW, Roell SA, et al. Three-dimensional proton MR spectroscopy of human prostate at 3 T without endorectal coil: feasibility. Radiology 2007;245:507–516. [PubMed: 17848681]

[43]. Zakian KL, Sircar K, Hricak H, et al. Correlation of proton MR spectroscopic imaging with Gleason score based on step-section pathologic analysis after radical prostatectomy. Radiology 2005;234:804–814. [PubMed: 15734935]

[44]. Kobus T, Vos PC, Hambrock T, et al. Prostate cancer aggressiveness: in vivo assessment of MR spectroscopy and diffusion-weighted imaging at 3 T. Radiology 2012;265:457–46. [PubMed: 22843767]

[45]. Yu KK, Scheidler J, Hricak H, et al. Prostate cancer: prediction of extracapsular extension with endorectal MR imaging and three-dimensional proton MR spectroscopic imaging. Radiology 1999;213:481–488. [PubMed: 10551230]

[46]. Ocak I, Bernardo M, Metzger G, et al. Dynamic contrast-enhanced MRI of prostate cancer at 3 T: a study of pharmacokinetic parameters. AJR Am J Roentgenol 2007;189:849. [PubMed: 17885055]

[47]. Kozlowski P, Chang SD, Jones EC, Berean KW, Chen H, Goldenberg SL. Combined diffusion-weighted and dynamic contrast-enhanced MRI for prostate cancer diagnosis-correlation with biopsy and histopathology. J Magn Reson Imaging 2006;24:108–113. [PubMed: 16767709]

[48]. Nicholson B, Schaefer G, Theodorescu D. Angiogenesis in prostate cancer: biology and therapeutic opportunities. Cancer Metastasis Rev 2001;20:297–319. [PubMed: 12085968]

[49]. Concato J, Jain D, Li WW, et al. Molecular markers and mortality in prostate cancer. BJU Int 2007;100:1259–1263. [PubMed: 17850375]

[50]. Noworolski SM, Vigneron DB, Chen AP, Kurhanewicz J. Dynamic contrast-enhanced MRI and MR diffusion imaging to distinguish between glandular and stromal prostatic tissues. Magn Reson Imaging 2008;26:1071–1080. [PubMed: 18508221]

[51]. Tofts PS, Brix G, Buckley DL, et al. Estimating kinetic parameters from dynamic contrast-enhanced T(1)-weighted MRI of a diffusible tracer: standardized quantities and symbols. J Magn Reson Imaging 1999;10:223–232. [PubMed: 10508281]

[52]. Kayhan A, Fan X, Oto A. Dynamic contrast-enhanced magnetic resonance imaging in prostate cancer. Top Magn Reson Imaging 2009;20:105–111. [PubMed: 20010065]

[53]. Puech P, Potiron E, Lemaitre L, et al. Dynamic contrast-enhanced magnetic resonance imaging evaluation of intraprostatic prostate cancer: correlation with radical prostatectomy specimens. Urology 2009;74:1094–1099. [PubMed: 19773038]

[54]. Lemaitre L, Puech P, Poncelet E, et al. Dynamic contrast-enhanced MRI of anterior prostate cancer: morphometric assessment and correlation with radical prostatectomy findings. Eur Radiol 2009;19:470–480. [PubMed: 18758786]

[55]. Cornud F, Beuvon F, Thevenin F, et al. Quantitative dynamic MRI and localization of non-palpable prostate cancer. Prog Urol 2009;19:401–413. [PubMed: 19467459]

[56]. Pinto F, Totaro A, Palermo G, et al. Imaging in prostate cancer staging: present role and future perspectives. Urol Int 2012;88:125–136. [PubMed: 22286304]

[57]. Bloch BN, Furman-Haran E, Helbich TH, et al. Prostate cancer: accurate determination of extracapsular extension with high-spatial resolution dynamic contrast-enhanced and T2-weighted MR imaging-initial results. Radiology 2007;245:176–185. [PubMed: 17717328]

[58]. Ogura K, Maekawa S, Okubo K, et al. Dynamic endorectal magnetic resonance imaging for local staging and detection of neurovascular bundle involvement of prostate cancer: correlation with histopathologic results. Urology 2001;57: 721–726. [PubMed: 11306390]

[59]. Takahashi N, Inoue T, Lee J, Yamaguchi T, Shizukuishi K. The roles of PET and PET/CT in the diagnosis and management of prostate cancer. Oncology 2007;72:226–233. [PubMed: 18176088]

[60]. Effert PJ, Bares R, Handt S, Wolff JM, Bull U, Jakse G. Metabolic imaging of untreated prostate cancer by positron emission tomography with 18fluorine-labeled deoxyglucose. J Urol 1996;155:994–998. [PubMed: 8583625]

[61]. Hofer C, Laubenbacher C, Block T, Breul J, Hartung R, Schwaiger M. Fluorine-18-fluorodeoxyglucose positron emission tomography is useless for the detection of local recurrence after radical prostatectomy. Eur Urol 1999;36:31–35.

[62]. Liu IJ, Zafar MB, Lai YH, Segall GM, Terris MK. Fluorodeox-yglucose positron emission tomography studies in diagnosis and staging of clinically organ-confined prostate cancer. Urology 2001;57:108–111. [PubMed: 11164153]

[63]. Kao PF, Chou YH, Lai CW. Diffuse FDG uptake in acute prostatitis. Clin Nucl Med 2008;33:308–310. [PubMed: 18356681]

[64]. Jadvar H, Ye W, Groshen S, Conti PS. F-18-fluorodeoxyglucose PET-CT of the normal prostate gland. Ann Nucl Med 2008;22:787–793. [PubMed: 19039557]

[65]. Minamimoto R, Uemura H, Sano F, et al. The potential of FDG-PET/CT for detecting prostate cancer in patients with an elevated serum PSA level. Ann Nucl Med 2011;25:21–27. [PubMed: 20931305]

[66]. Shiiba M, Ishihara K, Kimura G, et al. Evaluation of primary prostate cancer using 11C-methionine-PET/CT and 18F-FDG-PET/CT. Ann Nucl Med 2012;26:138–145. [PubMed: 22069194]

[67]. Yoshimoto M, Waki A, Yonekura Y, et al. Characterization of acetate metabolism in tumor cells in relation to cell proliferation: acetate metabolism in tumor cells. Nucl Med Biol 2001;28:117–122. [PubMed: 11295421]

[68]. Oyama N, Akino H, Kanamaru H, et al. 11C-acetate PET imaging of prostate cancer. J Nucl Med 2002;43:181–186. [PubMed: 11850482]

[69]. Kato T, Tsukamoto E, Kuge Y, et al. Accumulation of [11C]acetate in normal prostate and benign prostatic hyperplasia: comparison with prostate cancer. Eur J Nucl Med Mol Imaging 2002;29:1492–1495. [PubMed: 12397469]

[70]. Mena E, Turkbey B, Mani H, et al. 11C-Acetate PET/CT in localized prostate cancer: a study with MRI and histopathologic correlation. J Nucl Med 2012;53:538–545. [PubMed: 22343504]

[71]. Jambor I, Borra R, Kemppainen J, et al. Functional imaging of localized prostate cancer aggressiveness using 11C-acetate PET/CT and 1H-MR spectroscopy. J Nucl Med 2010;51: 1676–1683. [PubMed: 20956477]

[72]. Zeisel SH. Choline: an essential nutrient for humans. Nutrition 2000;16:669–671. [PubMed: 10906592]

[73]. Scher B, Seitz M, Albinger W, et al. Value of 11C-choline PET and PET/CT in patients with suspected prostate cancer. Eur J Nucl Med Mol Imaging 2007;34:45–53. [PubMed: 16932935]

[74]. Yamaguchi T, Lee J, Uemura H, et al. Prostate cancer: a comparative study of 11C-choline PET and MR imaging combined with proton MR spectroscopy. Eur J Nucl Med Mol Imaging 2005;32:742–748. [PubMed: 16052370]

[75]. Farsad M, Schiavina R, Castellucci P, et al. Detection and localization of prostate cancer: correlation of 11C-choline PET/CT with histopathologic step-section analysis. J Nucl Med 2005;46:1642–1649. [PubMed: 16204714]

[76]. Testa C, Schiavina R, Lodi R, et al. Prostate cancer: sextant localization with MR imaging, MR spectroscopy, and 11C-choline PET/CT. Radiology 2007;244:797–806. [PubMed: 17652190]

[77]. Martorana G, Schiavina R, Corti B, et al. 11C-choline positron emission tomography/computerized tomography for tumor localization of primary prostate cancer in comparison with 12-core biopsy. J Urol 2006;176:954–960. [PubMed: 16890665]

[78]. Beheshti M, Imamovic L, Broinger G, et al. 18F choline PET/CT in the preoperative staging of prostate cancer in patients with intermediate or high risk of extracapsular disease: a prospective study of 130 patients. Radiology 2010;254:925–933. [PubMed: 20177103]

[79]. Sutinen E, Nurmi M, Roivainen A, et al. Kinetics of [(11)C] choline uptake in prostate cancer: a PET study. Eur J Nucl Med Mol Imaging 2004;31:317–324. [PubMed: 14628097]

[80]. Igerc I, Kohlfürst S, Gallowitsch HJ, et al. The value of 18F-choline PET/CT in patients with elevated PSA-level and negative prostate needle biopsy for localisation of prostate cancer. Eur J Nucl Med Mol Imaging 2008;35:976–983. [PubMed: 18188560]

[81]. Giovacchini G, Picchio M, Coradeschi E, et al. (11)C-choline uptake with PET/CT for the initial diagnosis of prostate cancer: relation to PSA levels, tumour stage and anti-androgenic therapy. Eur J Nucl Med Mol Imaging 2008;35:1065–1073. [PubMed: 18200444]

[82]. Breeuwsma AJ, Pruim J, Jongen MM, et al. In vivo uptake of [11C]choline does not correlate with cell proliferation in human prostate cancer. Eur J Nucl Med Mol Imaging 2005;32:668–673. [PubMed: 15765234]

[83]. Rinnab L, Simon J, Hautmann RE, et al. [C11]choline PET/CT in prostate cancer patients with biochemical recurrence after radical prostatectomy. World J Urol 2009;27:619–625. [PubMed: 19234708]

[84]. Castellucci P, Fuccio C, Nanni C, et al. Influence of trigger PSA and PSA kinetics on 11C-choline PET/CT detection rate in patients with biochemical relapse after radical prostatectomy. J Nucl Med 2009;50:1394–1400. [PubMed: 19690023]

[85]. Richter JA, Rodriguez M, Rioja J, et al. Dual tracer 11C-choline and FDG-PET in the diagnosis of biochemical prostate cancer relapse after radical treatment. Mol Imaging Biol 2010;12: 210–217. [PubMed: 19543774]

[86]. Shiiba M, Ishihara K, Kimura G, et al. Evaluation of primary prostate cancer using 11C-methionine-PET/CT and 18F-FDG-PET/CT. Ann Nucl Med 2012;26:138–145. [PubMed: 22069194]

[87]. Nunez R, Macapinlac HA, Yeung HW, et al. Combined 18F-FDG and 11C-methionine PET scans in patients with newly progressive metastatic prostate cancer. J Nucl Med 2002;43:46–55. [PubMed: 11801702]

[88]. Schuster DM, Votaw JR, Nieh PT, et al. Initial experience with the radiotracer anti-1-amino-3–18F-fluorocyclobutane-1-carboxylic acid with PET/CT in prostate carcinoma. J Nucl Med 2007;48:56–63. [PubMed: 17204699]

[89]. Schuster DM, Taleghani PA, Nieh PT, et al. Characterization of primary prostate carcinoma by anti-1-amino-2-[18F]-fluo-rocyclobutane-1-carboxylic acid (anti-3-[18F] FACBC) uptake. Am J Nucl Med Mol Imaging 2013;3:85–96. [PubMed: 23342303]

[90]. Turkbey B, Mena E, Adler S, et al. GE-148 (18F) injection PET/CT imaging and multiparametric MRI for detection of localized prostate cancer using customized MRI-based specimen molds. J Nucl Med 2011;52:1906.

[91]. Schuster DM, Savir-Baruch B, Nieh PT, et al. Detection of recurrent prostate carcinoma with anti-1-amino-3–18F-fluo-rocyclobutane-1-carboxylic acid PET/CT and 111In-capromab pendetide SPECT/CT. Radiology 2011;259:852–861. [PubMed: 21493787]

[92]. Thomas CT, Bradshaw PT, Pollock BH, et al. Indrnm-111-cap-romab pendetide radioimmunoscintigraphy and prognosis for durable biochemical response to salvage radiation therapy in men after failed prostatectomy. J Clin Oncol 2003;21: 1715–1721. [PubMed: 12721246]

[93]. Barrett JA, LaFrance N, Coleman RE, et al. Targeting metastatic prostate cancer [PCa] in patients with 123I-MIP1072 and 123I-MIP1095 [abstract]. J Nucl Med 2009;50(Suppl. 2):522.

[94]. Cho SY, Gage KL, Mease RC, et al. Biodistribution, tumor detection, and radiation dosimetry of 18F-DCFBC, a low-molecular-weight inhibitor of prostate-specific membrane antigen, in patients with metastatic prostate cancer. J Nucl Med 2012;53:1883–1891. [PubMed: 23203246]

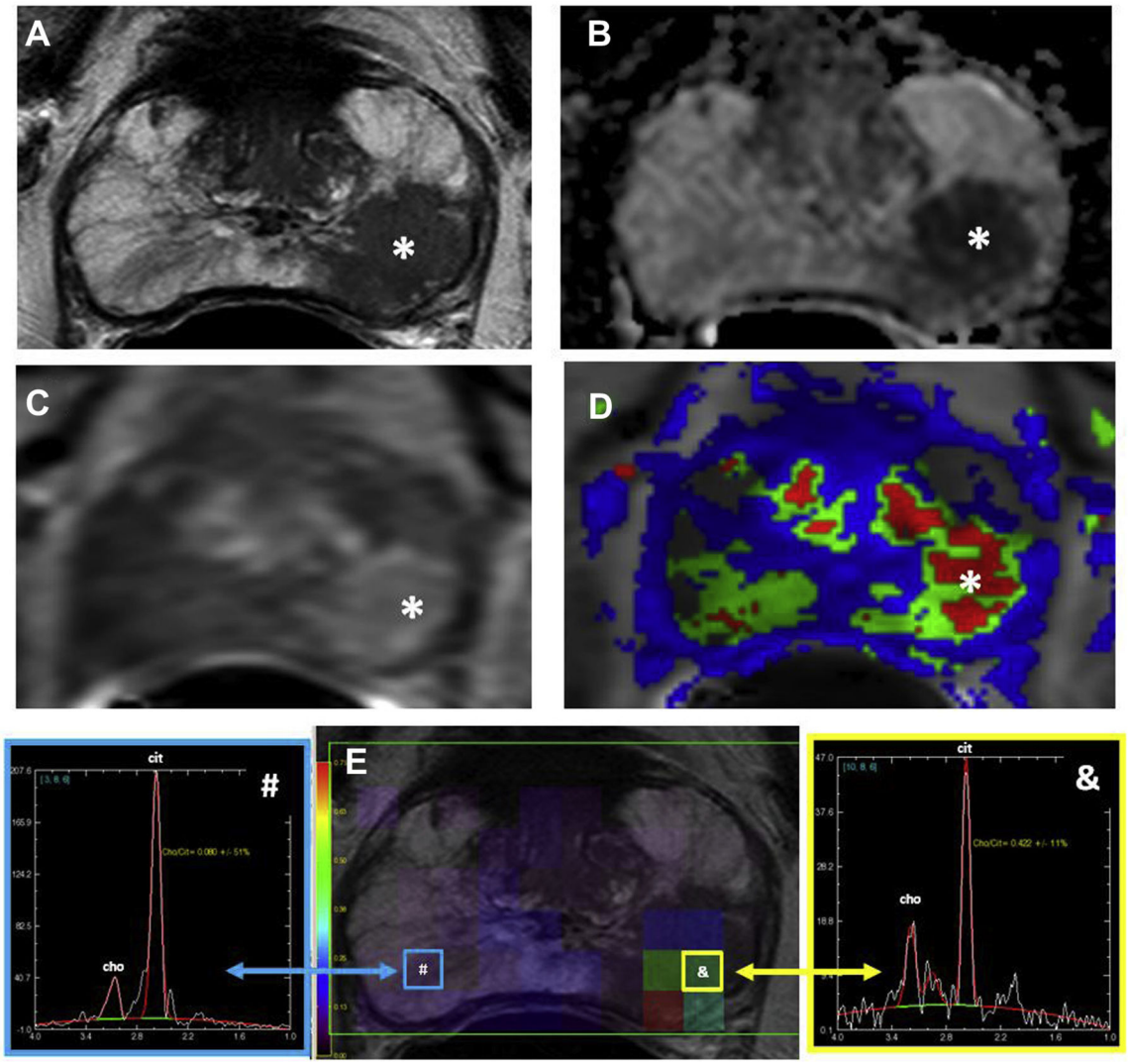

Fig 1.

A 63-year-old man with a serum prostate-specific antigen (PSA) of 14 ng/dl. (A) Axial T2-weighted magnetic resonance imaging (MRI), (B) apparent diffusion coefficient map of diffusion-weighted MRI, (C) raw dynamic contrast-enhanced (DCE) MRI and (D) K^{trans} maps derived from DCE MRI show a lesion in the left mid-peripheral zone (asterisk). (E) Magnetic resonance spectroscopy shows an elevated choline/citrate ratio in the left mid-peripheral zone compared with the normal right side. Subsequent transrectal ultrasound (TRUS)/MRI fusion-guided biopsy revealed a Gleason 4 + 4 (65%) tumour within that lesion.

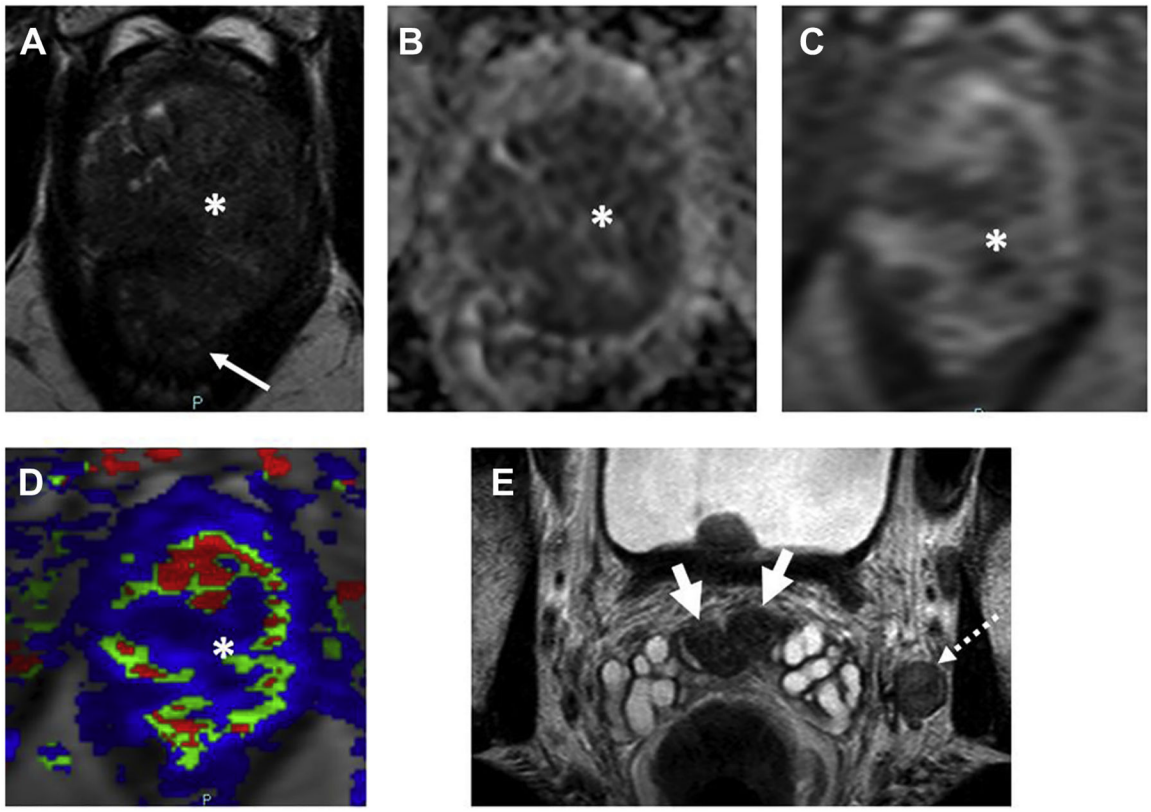

Fig 2.

A 52-year-old man with a serum prostate-specific antigen (PSA) of 23 ng/dl with no previous biopsy. (A) Axial T2-weighted magnetic resonance imaging (MRI), (B) apparent diffusion coefficient map of diffusion-weighted MRI, (C) raw dynamic contrast-enhanced (DCE) MRI and (D) K^{trans} map derived from DCE MRI show a lesion affecting almost the whole prostate gland (asterisk). The large lesion invades the rectum [(arrow in (A)] and seminal vesicles bilaterally [short arrows in (E)]. Additionally, a metastatic lymph node is present in the left obturator chain [dashed arrow in (E)]. Subsequent TRUS/MRI fusion-guided biopsy revealed a Gleason 5 + 5 tumour within the prostate.

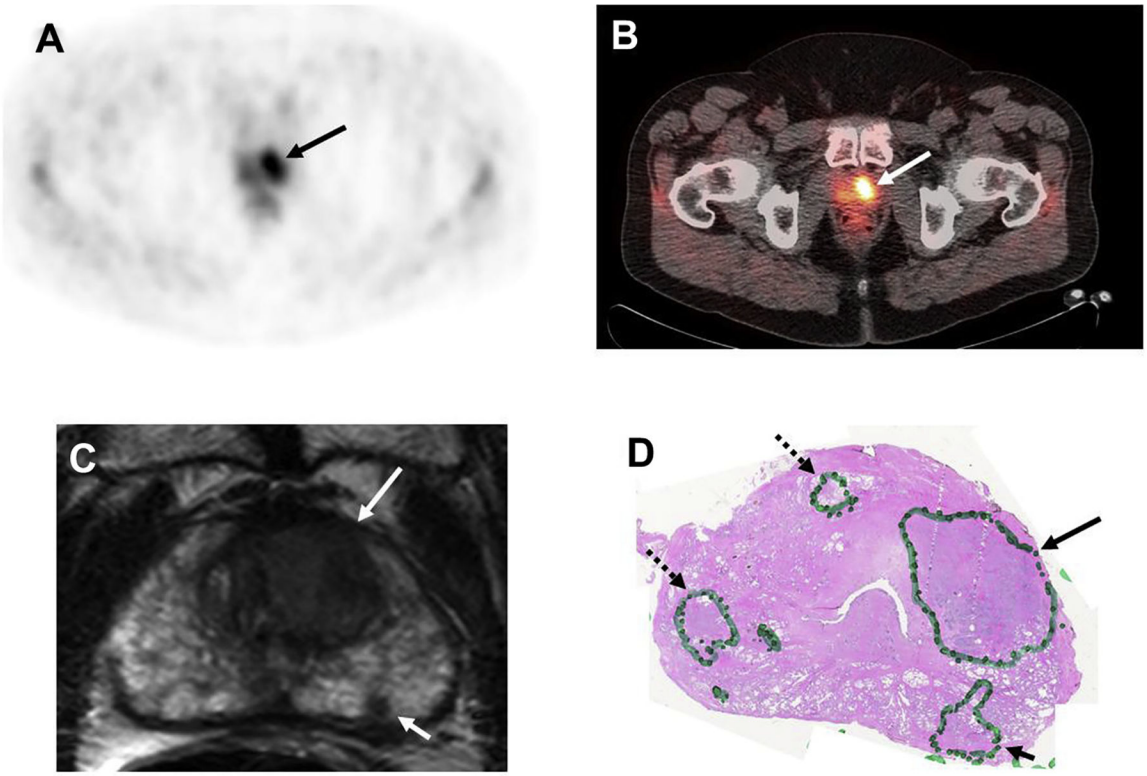

Fig 3.

A 59-year-old man with a prostate-specific antigen (PSA) of 8.6 ng/mL. ^{11}C-acetate positron emission tomography (PET) shows significant tracer uptake in the left-sided lesion on (A) PET and (B) PET/computed tomography images (arrows). (C) Axial T2-weighted magnetic resonance imaging (MRI) shows two lesions (large arrow: left anterior transitional zone; small arrow: left peripheral zone) in the left apical portion of the prostate. (D) Histopathology confirmed the presence of a Gleason 4 + 4 tumour within the left-sided large transitional zone lesion (arrow) and three smaller Gleason 3 + 3 lesions (dashed arrow lesions were missed by both ^{11}C-acetate PET and MRI, whereas the solid arrow lesion was detected by MRI only).